Electronic Supplementary Material for CrystEngComm

Co-crystallising Two Functional Complex Molecules in a Terpyridine Embrace Lattice

Clare A. Tovee,[a] Colin A. Kilner,[a] James A. Thomas[b] and Malcolm A. Halcrow*[a]

[a]*School of Chemistry, University of Leeds, Woodhouse Lane, Leeds, UK LS2 9JT. E-mail: m.a.halcrow@leeds.ac.uk*
[b]*Department of Chemistry, University of Sheffield, Sheffield, UK S3 7HF*

Electronic Supplementary Information

Experimental details for the crystal structure determinations

Figure S1 View of the complex dications in $[Fe(bpp)_2][BF_4]_2$ (left) and $[Ru(terpy)_2][BF_4]_2$.

Table S1 Selected bond lengths and angles in the crystal structures in this work.

Figure S2 Full ^{1}H NMR spectrum of a solution of $[Fe(bpp)_2][BF_4]_2$ and $[Ru(terpy)_2][BF_4]_2$ in CD_3NO_2.

Figure S3 Diamagnetic region of the ^{1}H NMR spectrum of a solution of $[Fe(bpp)_2][BF_4]_2$ and $[Ru(terpy)_2][BF_4]_2$ in CD_3NO_2, run 1 hr and 7 days after mixing.

Figure S4 Comparison of the room-temperature powder diffraction data for $[Fe(bpp)_2][BF_4]_2$, $[Ru(terpy)_2][BF_4]_2$ and two $[Fe(bpp)_2]_x[Ru(terpy)_2]_{1-x}[BF_4]_2$ compositions.

Table S2 Predicted and observed values of $\chi_M T$ (cm^3 mol^{-1} K) in the high and low-spin materials, based on the analytical compositions of the samples.

Figure S5 Warming mode magnetic data for $[Fe(bpp)_2]_x[Ru(terpy)_2]_{1-x}[BF_4]_2$, replotted as a function of the high-spin fraction of the material *vs.* T to highlight the unusual variation of $T_{½}$ with composition.

Figure S6 Emission spectra of solid $[Fe(bpp)_2]_x[Ru(terpy)_2]_{1-x}[BF_4]_2$ at 77 K.

Figure S7 Selected powder diffraction data from the $[Fe_yNi_{1-y}(bpp)_2][BF_4]_2$ compounds in this work.

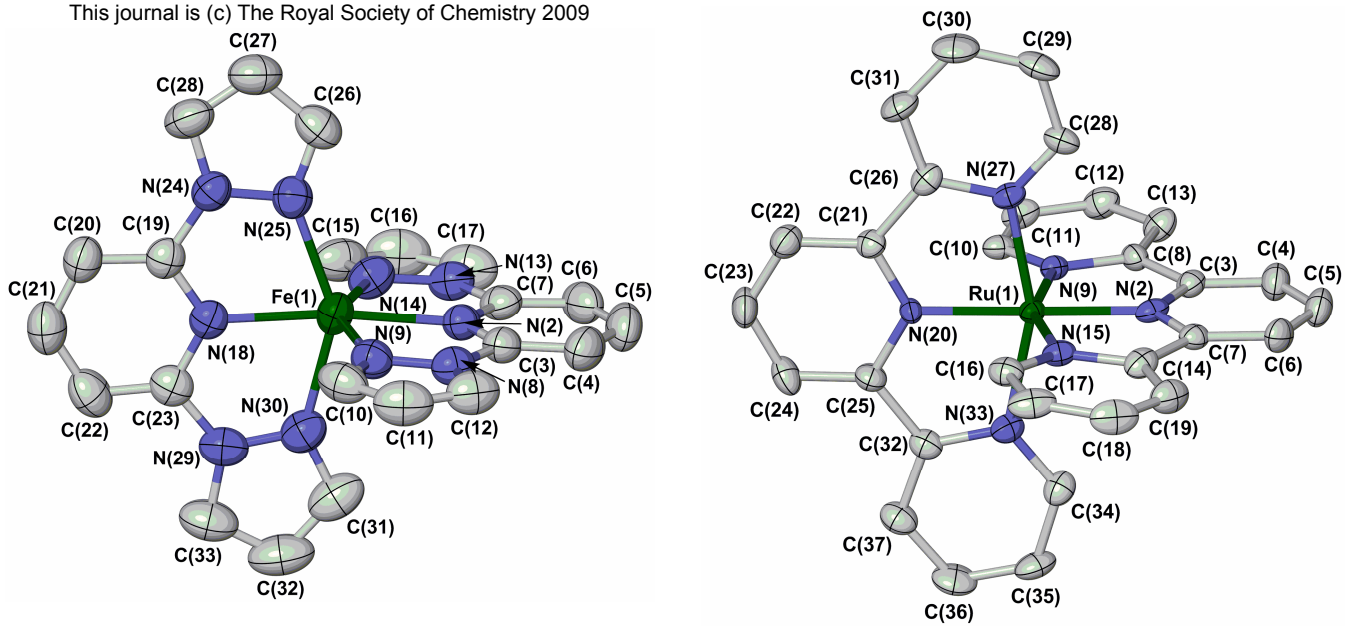

Fig. S1 View of the complex dications in $[Fe(bpp)_2][BF_4]_2$ (left) and $[Ru(terpy)_2][BF_4]_2$ (right), showing the full atom numbering scheme employed. All H atoms have been omitted for clarity, and thermal ellipsoids are at the 50% probability level.

Table S1 Selected bond lengths and angles in the crystal structures in this work (Å, °).

$[Fe(bpp)_2][BF_4]_2$ (high spin, from $MeNO_2/Et_2O$)		$[Ru(terpy)_2][BF_4]_2$	
Fe(1)–N(2)	2.1464(18)	Ru(1)–N(2)	1.999(8)
Fe(1)–N(9)	2.205(2)	Ru(1)–N(9)	2.098(4)
Fe(1)–N(14)	2.176(2)	Ru(1)–N(15)	2.092(5)
Fe(1)–N(18)	2.1444(19)	Ru(1)–N(20)	2.017(7)
Fe(1)–N(25)	2.192(2)	Ru(1)–N(27)	2.099(5)
Fe(1)–N(30)	2.190(3)	Ru(1)–N(33)	2.102(5)
N(2)–Fe(1)–N(9)	73.15(8)	N(2)–Ru(1)–N(9)	78.9(3)
N(2)–Fe(1)–N(14)	73.70(8)	N(2)–Ru(1)–N(15)	78.5(3)
N(2)–Fe(1)–N(18)	173.18(10)	N(2)–Ru(1)–N(20)	178.9(4)
N(2)–Fe(1)–N(25)	113.43(9)	N(2)–Ru(1)–N(27)	100.5(2)
N(2)–Fe(1)–N(30)	100.11(9)	N(2)–Ru(1)–N(33)	101.3(2)
N(9)–Fe(1)–N(14)	146.80(9)	N(9)–Ru(1)–N(15)	157.38(18)
N(9)–Fe(1)–N(18)	104.67(8)	N(9)–Ru(1)–N(20)	100.0(2)
N(9)–Fe(1)–N(25)	98.69(8)	N(9)–Ru(1)–N(27)	91.94(17)
N(9)–Fe(1)–N(30)	92.86(8)	N(9)–Ru(1)–N(33)	93.68(18)
N(14)–Fe(1)–N(18)	108.06(8)	N(15)–Ru(1)–N(20)	102.6(2)
N(14)–Fe(1)–N(25)	95.93(9)	N(15)–Ru(1)–N(27)	91.49(18)
N(14)–Fe(1)–N(30)	91.19(9)	N(15)–Ru(1)–N(33)	91.38(18)
N(18)–Fe(1)–N(25)	73.16(9)	N(20)–Ru(1)–N(27)	79.3(2)
N(18)–Fe(1)–N(30)	73.40(9)	N(20)–Ru(1)–N(33)	78.9(2)
N(25)–Fe(1)–N(30)	146.39(9)	N(27)–Ru(1)–N(33)	158.17(18)

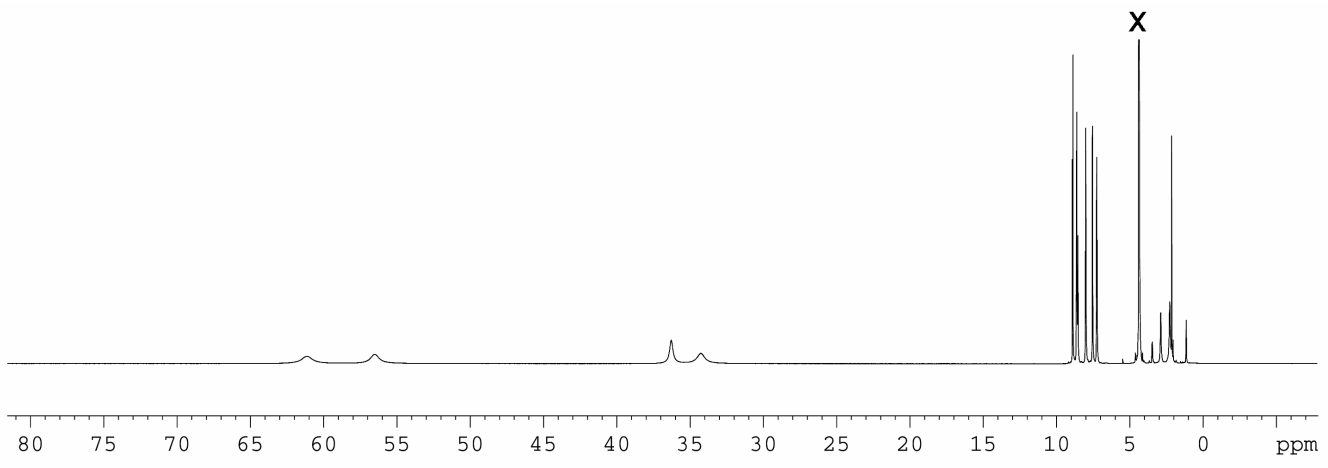

Figure S2 Full ^{1}H NMR spectrum of a solution of $[Fe(bpp)_2][BF_4]_2$ and $[Ru(terpy)_2][BF_4]_2$ in CD_3NO_2, taken 1 hr after mixing, showing a mixture of paramagnetic peaks from the iron complex and diamagnetic peaks from the ruthenium compound.

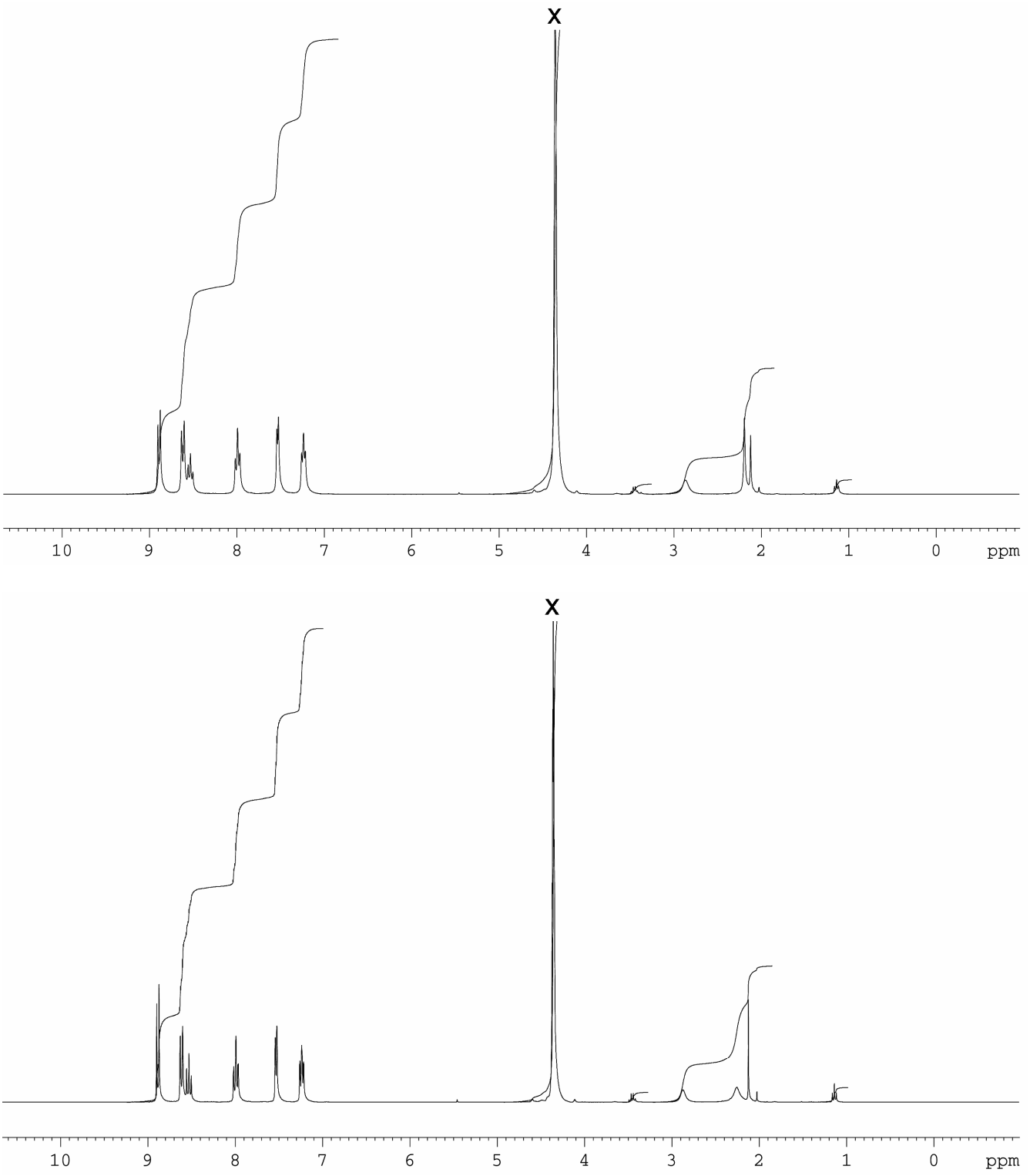

Figure S3 Diamagnetic region of the ^{1}H NMR spectrum of the same solution of $[Fe(bpp)_2][BF_4]_2$ and $[Ru(terpy)_2][BF_4]_2$ in CD_3NO_2, run 1 hr (top) and 7 days (bottom) after mixing. The identical nature of these spectra shows that bpp and terpy ligand exchange between iron and ruthenium centres does not take place on this timescale.

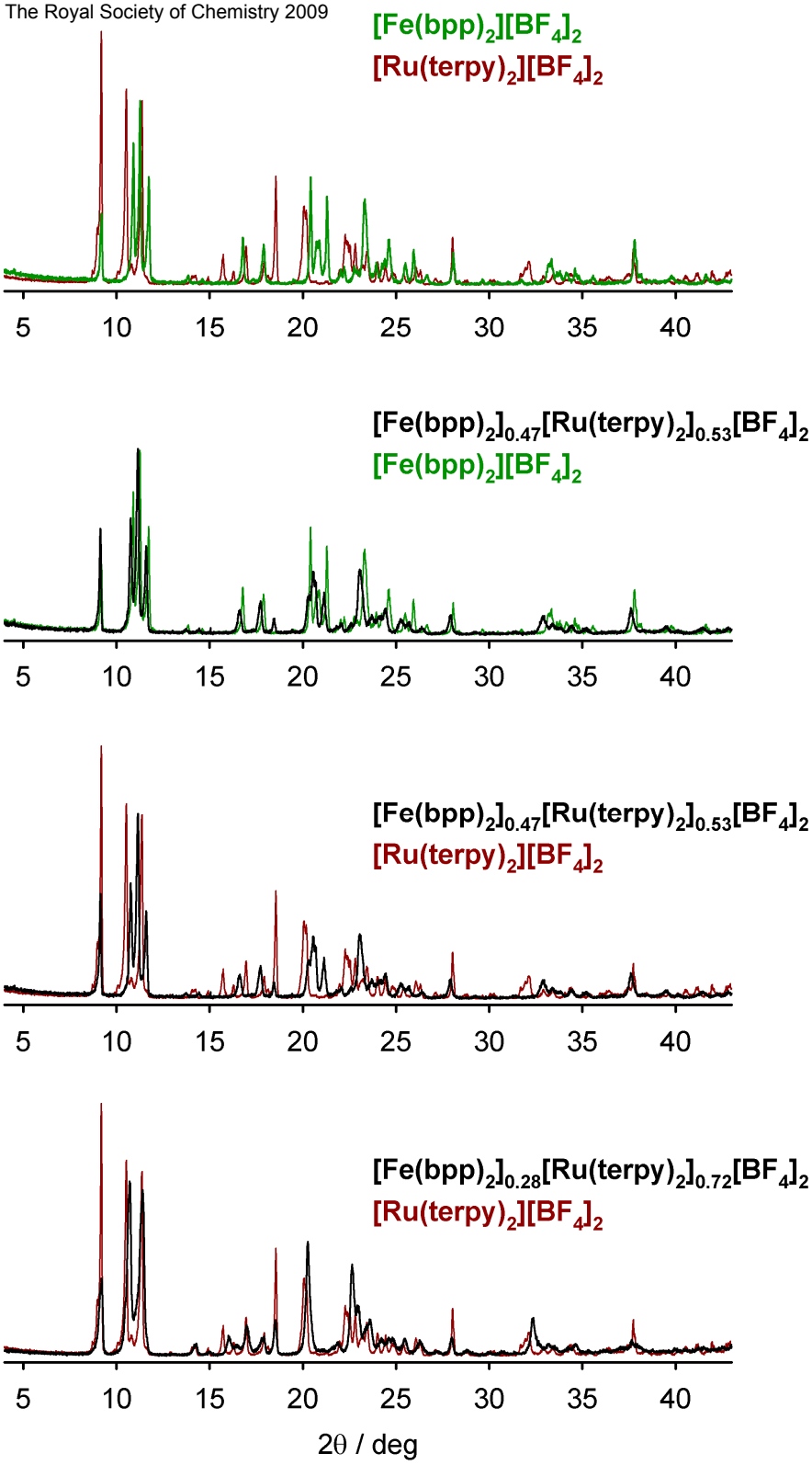

Figure S4 Comparison of the room-temperature powder diffraction data for pure $[Fe(bpp)_2][BF_4]_2$ (green), pure $[Ru(terpy)_2][BF_4]_2$ (red), and two $[Fe(bpp)_2]_x[Ru(terpy)_2]_{1-x}[BF_4]_2$ compositions (black).

The $[Fe(bpp)_2][BF_4]_2$ and $[Ru(terpy)_2][BF_4]_2$ powder patterns are clearly distinguishable (top), and data from $[Fe(bpp)_2]_{0.47}[Ru(terpy)_2]_{0.53}[BF_4]_2$ match for the $[Fe(bpp)_2][BF_4]_2$ structure much more closely than the $[Ru(terpy)_2][BF_4]_2$ structure (the two centre graphs). The weak diffraction peak at $2\theta = 18°$ in the solid solution, that does not have an obvious partner in the data from the iron complex, is evidence for contamination by a fraction of the *Cc* phase however. In contrast, data from $[Fe(bpp)_2]_{0.28}[Ru(terpy)_2]_{0.72}[BF_4]_2$ are a close match for pure $[Ru(terpy)_2][BF_4]_2$ (bottom).

Table S2 Predicted and observed values of $\chi_M T$ ($cm^3\ mol^{-1}\ K$) from the high- and low-spin samples, based on the analytical compositions of the samples. The calculations use the following $\chi_M T$ values for the pure components of the solid solutions; high-spin $[Fe(bpp)_2][BF_4]_2$, = 3.5; low-spin $[Fe(bpp)_2][BF_4]_2$, 0; $[Ru(terpy)_2][BF_4]_2$, 0; $[Ni(bpp)_2][BF_4]_2$, 1.2.

$[Fe(bpp)_2]_x[Ru(terpy)_2]_{1-x}[BF_4]_2$

x	Low-spin (calc)	T = 50K (obs)	High-spin (calc)	T = 340K (obs)
0.95	0	0.06	3.33	3.36
0.75	0	0.01	2.63	2.52
0.57	0	0.02	1.99	1.93
0.47	0	0.02	1.65	1.59
0.28	0	0.02	0.98	0.88

$[Fe_yNi_{1-y}(bpp)_2][BF_4]_2$

y	Low-spin (calc)	T = 50K (obs)	High-spin (calc)	T = 300K (obs)
0.95	0.06	0.07	3.39	3.36
0.83	0.20	0.18	3.11	3.21
0.68	0.38	0.38	2.76	2.65
0.50	0.60	0.61	2.36	2.21
0.30	0.84	0.82	1.87	1.71
0.15	1.02	1.03	1.56	1.49

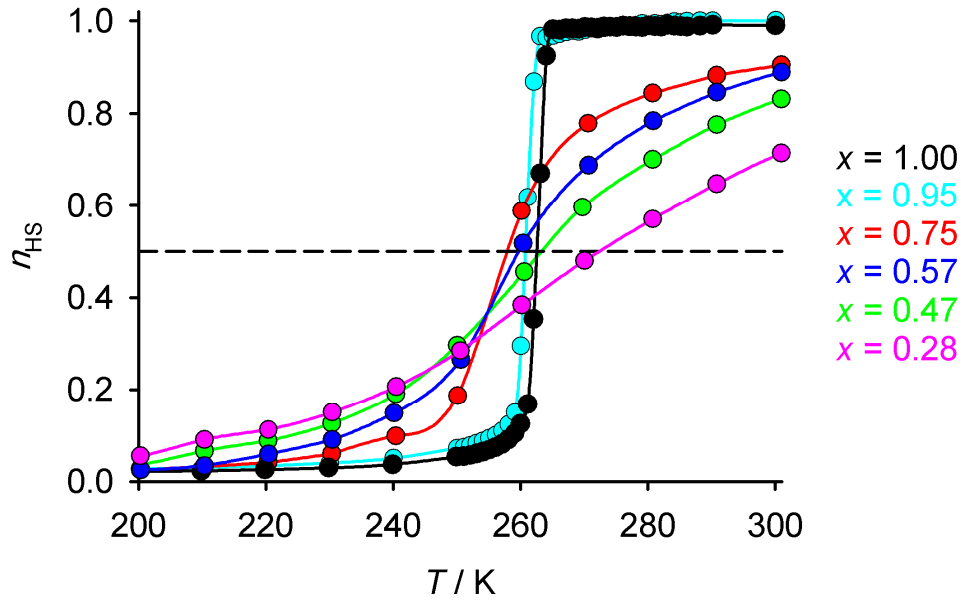

Figure S5 Warming mode magnetic data for $[Fe(bpp)_2]_x[Ru(terpy)_2]_{1-x}[BF_4]_2$, replotted as a function of the high-spin fraction of the material (n_{HS}) *vs.* T to highlight the unusual variation of $T_{½}$ with composition. The midpoint-fraction n_{HS} = 0.5 is highlighted with a dotted line, and the data points for each compound are linked with a simple spline curve for clarity.

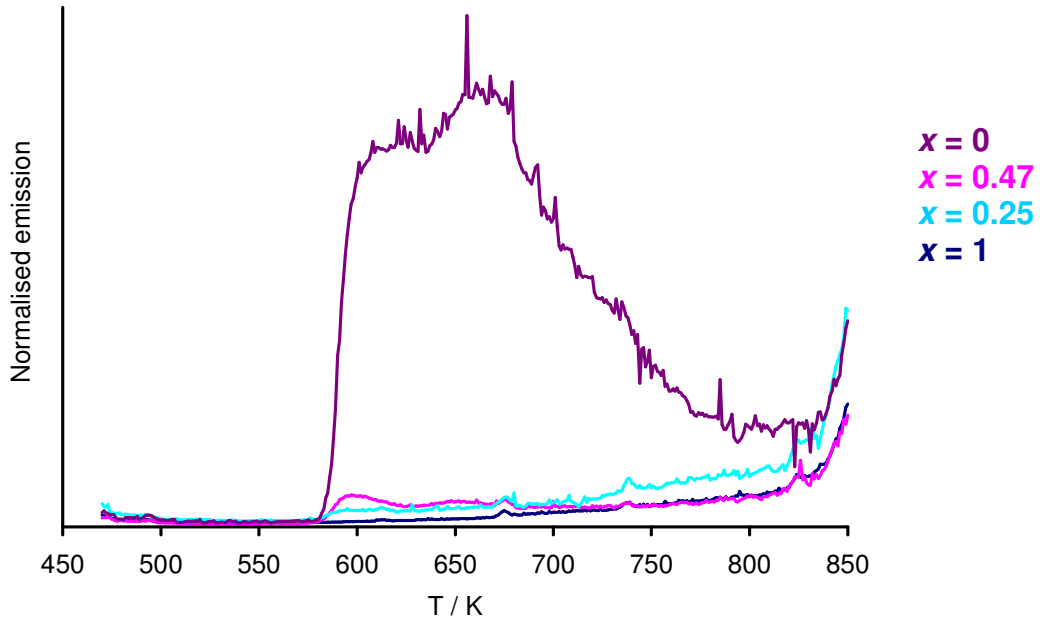

Figure S6 Emission spectra of selected solid $[Fe(bpp)_2]_x[Ru(terpy)_2]_{1-x}[BF_4]_2$ compounds at 77 K. All four spectra are plotted to the same vertical emission scale.

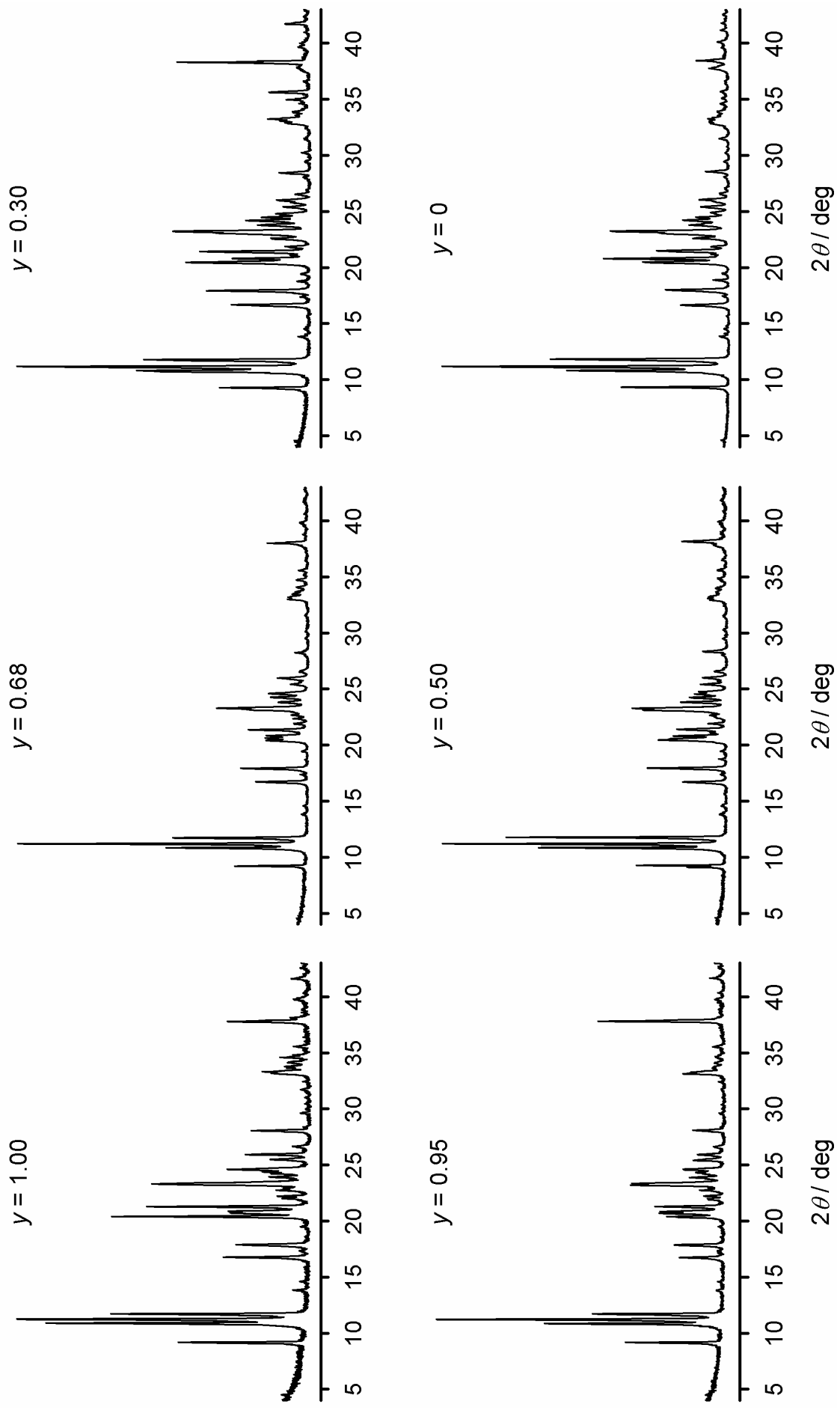

Figure S7 Selected powder diffraction data from the $[Fe_yNi_{1-y}(bpp)_2][BF_4]_2$ compounds in this work (298 K, Cu-$K\alpha$ radiation).